A 2D model of hydraulic fracturing, damage and microseismicity

Magnus Wangen

E-mail: Magnus.Wangen@ife.no

Institute for Energy Technology,
P.O.Box 40, N-2027 Kjeller, Norway

2017

Abstract

We present a model for hydraulic fracturing and damage of low permeable rock. It computes the intermittent propagation of rock damage, microseismic event locations, microseismic frequency-magnitude distributions, stimulated rock volume and the injection pressure. The model uses a regular 2D grid and is based on ideas from invasion percolation. All damaged and connected cells during a time step constitute a microseismic event, where the size of the event is the number of cells in the cluster. The magnitude of the event is the $\log_{10}$ of the event size. The model produces events with a magnitude frequency distribution having a b value that is approximately 0.8. The model is studied with respect to the physical parameters: permeability of damaged rock and the rock strength. "High" permeabilities of the damaged rock give the same b value ≈ 0.8, but "moderate" permeabilities give higher b values. Another difference is that "high" permeabilities produce a percolation-like fracture network, while "moderate" permeabilities result in damage zones that expand circularly away from the injection point. In the latter case of "moderate" permeabilities, the injection pressure increases substantially beyond the fracturing level. The rock strength and the time step do not change the observed b value of the model for moderate changes.

Keywords: Hydraulic fracturing, rock damage, microseismicity

1 Introduction

Shales are tight rocks with a permeability that is normally less than 10^{-19} m^2, which means that they are almost impermeable (Neuzil, 1994). Therefore, it is practically impossible to inject into or produce pore fluids from shales. The injection of fluid under high pressure can fracture and damage the shales and may create a fracture network that allows the fluid to enter the rock matrix. The fluid pressure has to exceed the least compressive stress in order to drive the damage process and open the rock for fluid flow (Zoback, 2010). The fracture network has to be pervasive in order to enable the shales to produce substantial quantities of pore fluids such as gas and oil (Norris et al., 2016). The hydraulic fractured and damaged shales can therefore be attributed an effective permeability. The term damaged is used to denote a complex fracture network, which is both coarse and fine and fills a rock volume (Busetti et al., 2012b,a).

If the hydraulic fracturing process had created a planar fracture, which may be the result of hydraulic fracturing, it would not have been possible to inject fluid into the rock matrix or to produce pore fluids from the rock matrix (Norris et al., 2016). In the case of a planar fracture in a tight rock, all the injected fluid becomes stored inside the fracture, without any leak-off into the rock matrix. This is what happens during the formation of magmatic intrusions such as sills and dikes (Spence and Turcotte, 1985). The molten magma that fills the fractures remains there, solidifies and becomes a manifestation of the fracture geometry (Spence and Turcotte, 1985).

The physical processes involved with the hydraulic fracturing of shales and the associated production of the large quantities of oil and gas are poorly understood (Turcotte et al., 2014). There are indications that the shales suitable for oil and gas production by hydraulic fracturing have a carbonate cemented fracture network formed over a long geohistory (Norris et al., 2014b, 2016; Turcotte et al., 2014). The carbonate minerals have low strength, and the cemented fractures may be opened by the injection fluid under high pressure. The carbonate cemented fracture network is so fine that it gives access to the fine pores of the shales.

The aim of the current work is to demonstrate a modelling framework for the hydraulic fracture process that can produce realistic microseismicity and estimate the volume of damaged rock. The model builds on the loop-less invasion percolation model developed by Norris et al. (2014b,a), which is extended with a pressure equation. The model then allows for the simulation of microseismic events, where locations, microseismic frequency-magnitude distributions, stimulated rock volume and time variations in the injection pressure are properties in real space and

time, as opposed to a pure percolation model (Norris et al., 2014b,a).

This paper is organized as follows: A short review of different models producing microseismicity is given, the algorithm for hydraulic fracturing and rock damage is presented, and microseismic events and event sizes are explained. The numerical solution of the pressure equation is formulated and the stationary pressure solution is introduced. The numerical model is demonstrated, before magnitudes and frequency of events are reported.

2 Models producing microseismicity by fluid injection

There does not appear to be one standard approach to modelling the mechanical processes that generate microseismicity and the distribution of microseismic events. Instead, there are a number of quite different approaches. An important reason for the variety in approaches is the intermittent behaviour of the fracturing process, which is not handled by standard continuum mechanics. Continuum mechanics normally deal with processes that are smooth and well behaved in time and space. Another reason is that the intermittent nature of microseismicity can be represented in a number of different ways.

One of the first approaches that modelled the intermittent behaviour of a hydraulic fracturing was the beam model developed by Tzschichholz et al. (1994) and Tzschichholz and Herrmann (1995). The beam model is a representation of an impermeable solid matrix by a 2D regular grid of square cells, where four beams are welded together at each intersection. The beams, which are the cell sides, are assigned random strength in terms of strain. The beams along the fracture surface become stretched when fluid is injected into the fracture, and they will eventually break. The breaking can release a chain of broken beams, where clusters of broken beams become events. This modelling approach was later extended with leak-off and Darcy flow in the matrix by Tzschichholz and Wangen (1998). The beam model has evolved into finite element models for hydraulic fracturing, where the beam representation of the matrix is replaced by finite elements with Biot poroelastic properties (Wangen, 2011, 2013).

A different approach is taken by the Discrete Fracture Network (DFN) models, which consider fracturing and fluid flow in a predefined fracture network. An early example is the model suggested by Bruel and Charlety (2007) for simulation of the microseismicity induced by hydraulic fracturing at the geothermal site

Soultz sous Forêts in France. The DFN model uses a power law distribution of fracture sizes (Bruel, 2007). The matrix is assumed impermeable, and the fluid flow is restricted to the fracture network. The model is capable of modelling shear failure and realistic microseismic locations for an injection pressure that is less than the least compressive stress. A similar approach is used in the commercial tool UDEC (Itasca International, 2016), which simulates the propagation of fractures along predefined planes, where flow occurs in the fracture planes (Riahi and Damjanac, 2013).

The idea to populate a model with fractures with a given size distribution is applied in more complex models, where predefined fractures may break and release seismic energy. Izadi and Elsworth (2014) have seeded discrete penny-shaped fractures within the reservoir volume, where reservoir geochemistry and stress are modelled with the coupling of ToughReact and Flac3D simulators as demonstrated by Taron et al. (2009). The predefined or randomly seeded fractures may slip as the pore pressure increases due to fluid injection and thereby release microseismic events. A similar approach is taken by Verdon et al. (2015), where the locations, orientations and sizes of pre-existing fractures in the In Salah reservoir are reconstructed using a geomechanical model. A Mohr-Coulomb fracture condition is used to determine if the modelled stress triggers shear failure and fault slip. The modelling approaches taken by Izadi and Elsworth (2014) and Verdon et al. (2015) lead to complex models, which involves a number of assumptions and associated parameters.

A simpler approach to the modelling of microseismic events is taken by Rothert and Shapiro (2003), where they are assigning a random critical fluid pressure to each cell in a numerical grid. A parabolic pressure equation is solved numerically with the finite element method assuming a homogeneous background diffusivity, where the pressure distribution is driven by a point source for fluid. Whenever the pressure in a cell exceeds the critical pressure a microseismic event is triggered. The model gives realistic locations in space and time, but there is no feedback from the seismic events on the permeability. The model produces a seismic cloud that expands in accordance with analytical models (Shapiro et al., 2006), although it does not produce a microseismic size distribution. Langenbruch and Shapiro (2014) found that a Gutenberg-Richter relation for the microseismic events results from a power-law size distribution of the fracture surface area.

Microseismicity, like seismicity, is observed as events with frequencies and magnitudes that follow a power law distribution (Baan et al., 2013). A wide range of natural phenomena are observed to have event sizes with a power-law distribution (Turcotte, 1997). Examples of models for such phenomena are the sand pile model (Bak et al., 1987), earthquake models (Crampin and Gao, 2015), nat-

ural hydraulic fracturing (Miller and Nur, 2000), pore throat models for immiscible displacement in porous media (Furuberg et al., 1988; Aker et al., 1998) and acoustic emissions by triaxial testing of rocks (Amitrano, 2003, 2012). A key to the modelling of event size distributions with a regular grid of cells is that the model can produce bursts of single cell events, which may be triggered when one cell becomes critical. The triggering of a single event leads to the redistribution of excess mass or energy with neighbour cells, which in turn may become critical, and in this way may set off an avalanche of single cell events. A connected cluster of neighbour cells is a main event, where the number of cells in the main event is the event size.

Norris et al. (2014b,a) have suggested an invasion percolation model that produces realistic micro-seismic event size distributions. Invasion percolation is a dynamic percolation process, which was introduced by Wilkinson and Willemsen (1983) to model the displacement of one fluid by another in a porous medium with capillary effects. The bonds in the 2D model represent pore throats, and they are assigned different capillary thresholds. Invasion percolation produces bursts (Furuberg et al., 1988, 1996). A burst results when the fluid overcomes a pore throat with a high capillary threshold and then has access to a number of new pores with the possibility of a lower capillary threshold. Norris et al. (2014b,a) make use of the same idea, where rock strength rather than capillary threshold, controls the invading fluid. Another difference is that there are no loops in the branching fracture structure produced by the invading fluid. The reason for this assumption is that the pressure difference across an unbroken bond between two fracture branches is too small to break the bond (Norris et al., 2014b,a).

3 An algorithm for hydraulic fracturing and rock damage

The model treats a 2D horizontal layer discretized with a regular grid of square cells. The centers of two nearest neighbour cells are connected by a transmissibility, also called a bond (see figure 1). The intact bonds initially have shale permeability. Fluid injection starts in the center cell of the grid. The center cell is initially assigned a high “damage” permeability. When injection starts the fluid pressure rises quickly in the initially damaged cell, which eventually leads to the damage of a new intact bond and the corresponding intact cell. The broken bond gets “damage” permeability, which allows the fluid to invade the newly damaged cell. It is only the intact bonds connected to the damaged cells that are subjected to an increasing fluid pressure. Therefore, only the intact bonds that lead from

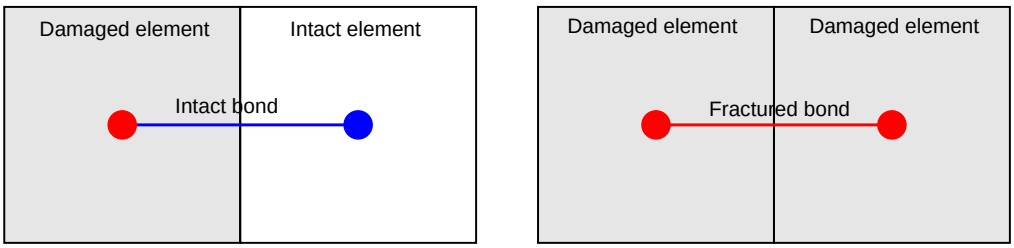

(a) (b)

Figure 1: *(a) The bonds that can be damaged are the ones that lead from a damaged element to an intact element. Only the damaged cells have an elevated fluid pressure due to injection. (b) When the bond becomes damaged, this implies that the intact cell also becomes damaged.*

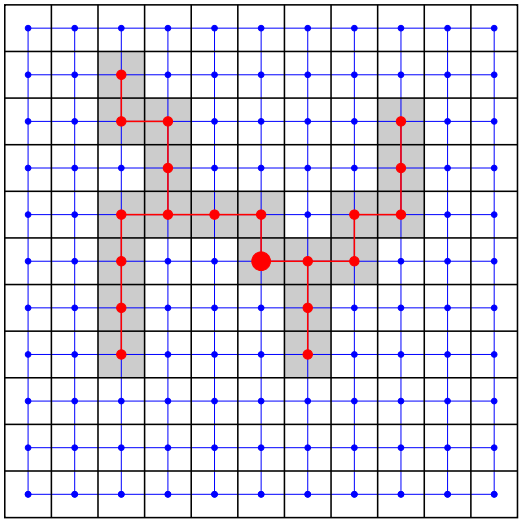

Figure 2: *The broken bonds form branching paths into the rock. There are no loops in the path, similar to loop-less invasion percolation, which means that there is at maximum two bonds, one bond into a cell and one out of the cell.*

damaged cells to intact cells can break, as illustrated in figure 1. Injection maintains a fluid pressure that propagates the damage into the intact rock, away from the injection cell, as shown in figure 2.

The grid is aligned with the principal stresses of the local horizontal stress field, where the local stress field may be anisotropic. A bond is compressed by the principal stress acting normal to its sides. Breaking of a bond happens when the fluid pressure exceeds the compressive stress of the bond plus the bond strength. This ensures that the damage process propagates normal to the least compressive stress in case of equal bond strength. The bond strengths are assigned random values, accounting for the heterogeneous nature of the shale. In the case examples presented later, the stress field is assumed isotropic in the plane, with the vertical stress as the largest principal stress.

Random bond strength is a simple representation of the strongly heterogeneous nature of rocks. This heterogeneity is due to depositional features such as variable grain size and mineral composition, but also features that are acquired during a long geohistory, such as a fracture network that is healed by precipitation of the mineral cement. Percolation models represent heterogeneity by normalized strength, which is simply the uniform distribution between 0 and 1. This model uses a uniformly distributed bond strength between zero and a maximum value. The introduction of a pressure equation and bond strength with units of Pa brings the ideas of a percolation model closer to real cases of hydraulic fracturing. For instance, the proposed model leads to predictions of damaged rock volume, injection pressure and microseismicity in real time and real space, results that can be compared with observations.

Propagation of one fracture is driven by the stress enhancement at its fracture tips. How the stress enhancement and fracture interaction control the propagation in heterogeneous rocks are studied numerically by several different approaches (Flekkøy et al., 2002; Niebling et al., 2012; Ghani et al., 2013; Wangen, 2011, 2013). These models have in common that they solve for the full stress field in the rock matrix, when a few fractures are explicitly represented. The damage approach to the hydraulic fracturing assumes that the number of fractures is so large and that they are so fine that it is practically impossible to represent each of them. The fracture propagation is assumed controlled by the strong heterogeneous nature of the rock, where interactions of microfractures take place on a length scale that is much less than the size of an element. The element size is typically several meters. Therefore, the bond fracture condition, which is based on the fluid pressure, is a simplification that ignores details of the fracture network. It represents two main aspects of the fracture process. First, the fluid pressure must exceed compressive stress in order to dilate the damaged rock and thereby

propagate the damaging. The second aspect is the impact of heterogeneities on the damage process.

The damage of rocks is associated with micro-crack nucleation and propagation (Amitrano, 2006). Once a bond is damaged, its transmissibility also changes from intact to damaged. The damage permeability allows the fluid to flow through the bond and invade the newly damaged cell. The dilation of the damaged zone by a fluid pressure exceeding the compressive stress leads to a pressure dependent permeability. Constant damage permeability is used as a simplification when the fluid pressure is larger than the least compressive stress.

Microseismic events have been differentiated as "wet" and "dry" events (Maxwell et al., 2015). The dry events are triggered by mechanical stress changes that do not directly involve the fluid pressure. On the other hand, the wet events are triggered by an increasing fluid pressure, which pushes a Mohr circle to the left until it touches a failure envelope and thereby creates a shear event (Maxwell et al., 2015). Hydraulic fracturing in low permeable rock is normally understood as being tensile, where the fluid pressure opens the fractures (Zoback, 2010). The microseismicity directly related to the tensile fracturing constitutes "wet" fractures. The actual fracturing process taking place in a heterogeneous shale with an anisotropic regional stress field may involve a combination of tensile fracturing, shear fracturing, damage and reopening of cemented fracture networks, where the fracturing is not localized to one or a few well-defined fracture planes.

4 Microseismic events and event sizes

Our numerical procedure is based on time stepping, where the pressure equation may need repeated solutions at each time step as long as there are critically pressured bonds. A time step begins with a numerical solution of the pressure equation. Several bonds may then be in a critical state, having a fluid pressure that exceeds the least compressive stress plus the bond strength. The most critical bond is selected and broken. The fluid can then invade a new cell, which implies that the next numerical solution for the fluid pressure becomes slightly reduced in the network of damaged cells. If there are still more critically stressed bonds with the new reduced pressure, then the most critical bond is broken, and the same procedure continues repeatedly until there are no more critical bonds. The pressure equation has to be resolved after each breaking of a bond in order to account for the newly damaged bond and cell in the fracture network.

The broken bonds and cells are counted and all connected broken cells during

a time step constitute a cluster, which forms a fracture or damage event. In the loop-less fracture network the number of broken bonds is the same as the number of broken cells. Breaking one bond always implies that one cell is also broken. It is these clusters that are the microseismic events, where the size of the event is the number of cells in the cluster. There are normally a few clusters with a large number of cells and a large number of small events, with just a few cells. The magnitude of the event is the $\log_{10}$ of the event size. The space location is the center of gravity of the cluster, and the current discrete time is the time location. The procedure is similar to how microseismicity is modelled with loop-less invasion percolation (Norris et al., 2014b,a), except that the addition of the pressure equation brings real space, real time and fluid pressure into the model.

5 Numerical solution for fluid pressure

Each breaking of a bond opens a new cell for fluid. A new solution of the pressure equation is therefore required to account for the pressure change that results from the fluid entering the new cell. The fluid pressure is governed by the following pressure equation

$$\phi\,\alpha(\mathbf{x})\frac{\partial p}{\partial t} - \nabla\cdot\Big(\frac{k(\mathbf{x})}{\mu}\nabla p\Big) = \begin{cases} q & \text{for the injection cell} \\ 0 & \text{otherwise} \end{cases}, \tag{1}$$

which accounts for the mass conservation in the damaged cells and the rock. The Appendix provides a derivation of equation (1) from the conservation of fluid mass and a definition of the effective compressibility. The symbol ϕ is porosity, $\alpha(\mathbf{x})$ is the effective compressibility, $k(\mathbf{x})$ is the permeability field, μ is the viscosity and p is the overpressure. The overpressure is the fluid pressure minus the hydrostatic pressure. There are large uncertainties related to the effective values of porosity, compressibility and permeability of the damaged rock. These parameters depend on the properties of the fracture network and how they are related to the fluid pressure. The pressure equation is simplified by using constant values for these properties, because of the uncertain nature of damaged rock. The permeability and the effective compressibility are the parameters that change for a cell that goes from intact rock to damaged rock. The transmissibility that connects a damaged cell with an intact cell is based on the harmonic mean of the permeabilities k_D for damaged rock and k_I for intact rock, respectively,

$$k_M = \frac{2}{1/k_D + 1/k_I}, \tag{2}$$

when the two cells are connected in series. The harmonic mean becomes dominated by the low permeable rock. The average is close to $k_M \approx 2K_I$, even if the

permeability of the damaged rock is larger than that of the intact rock by several orders of magnitude. The way in which the transmissibilities appear in the finite volume formulation is shown in the Appendix. The effective compressibility is α_I for intact rock and α_D for damaged rock.

Pressure equation (1) is discretized with a finite volume method, as shown in the Appendix. The initial pressure is hydrostatic and the external boundaries remain hydrostatic. Hydrostatic boundaries are the same as zero overpressure at the boundaries. Fluid is injected at a constant rate at the center cell of the grid. The default implementation solves for the pressure in every grid cell. This is a necessary approach for permeable rocks, where there is an important leak-off from the damaged cells into the intact cells. In case the intact cells have a shale permeability, there will be almost no leak-off from the damaged cells into the intact cells. It is not necessary, in this case, to solve for the pressure in the intact cells. The numerical solution can then be restricted to the damaged and permeable cells, since the fluid flow is restricted there. The intact cells retain their initial hydrostatic pressure until they are damaged. This approach allows for a numerical pressure solver that is much faster, but a little less straight forward to implement.

The approach of solving only for fluid flow in the damaged cells is therefore adopted, as the model is applied to intact rock with shale permeabilities. The boundary conditions are therefore zero overpressure in all the intact neighbour cells to the damaged cells. This approach becomes considerably faster since the number of damaged cells starts with the injection cell. Although the number of damaged cells grow, it will always be much less than the total number of cells in the grid. For example, in a grid with $500 \times 500 = 25000$ cells, where less than 2500 cells become damaged, this approach is at least 10 times faster than solving for the pressure in all the cells.

6 Stationary solution for fluid pressure

The algorithm can also be tested in the regime where the damaged rock permeability is sufficiently large for the pressure difference to be negligible between the injection cell and the most distant damaged cells. In this case, the overpressure is

$$p_{\text{apx}} = \frac{Q\,t}{\phi \alpha_D V_D}, \tag{3}$$

where V_D is the volume of the damaged cells. Then, all damaged cells have almost the same pressure, which is controlled by the compressibility, the volume of fluid

injected and the volume of damaged rock. The approximate solution (3) is the stationary solution of equation (1) after a volume $Q\,t$ has been injected, assuming no leak-off into the intact cells. The constant stationary pressure is the solution, after injection is stopped and all pressure transients have died out. The time needed for the transients to die out can be estimated with characteristic time

$$t_0 = \frac{1}{k_D}\phi\alpha_D\mu r_{\max}^2, \tag{4}$$

where $r_{\max}$ is the average radius of the damaged zone. For cases with a high damage permeability and almost no leak-off, it turns out that the numerical pressure solution for the injection cell, where the pressure is at maximum, is just slightly above the stationary solution (3). The pressure (3) is a good approximation, when the time constant t_0 for reaching a stationary state is short compared with the injection time, which is the case with high permeabilities for the damaged rock.

Even if the approximation (3) cannot always be used in the simulations it is still useful as a reference solution. The numerical solution will often be close to the approximate solution, even in cases where pressure transients are important. The solution (3) is also the average overpressure p_{av} in the damaged rock volume, and it can be used to estimate the bulk volume of damaged rock,

$$V_D = \frac{Q\,t}{\phi\alpha_D p_{\text{av}}}. \tag{5}$$

This is the stimulated bulk volume by the hydraulic fracturing process. This estimate is useful during injection as long as the permeabilities are high and $p_{\text{av}} \approx p_{\text{apx}}$. The volume of damaged rock can be used to estimate the radius of the damaged zone when it propagates radially away from the injection site. Setting $V_D = hr^2$ gives the radius

$$r(t) = \left(\frac{Qt}{\pi\phi\alpha_D p_{\text{av}} h}\right)^{1/2}, \tag{6}$$

as a function of time, where $h = 1$ m is the unit thickness of the 2D layer.

7 Numerical demonstration

The model behaviour depends on physical properties such as the damaged rock permeability and the bond strength, but it also depends on numerical parameters such as the time step and the grid resolution. The model is first demonstrated with

Parameter	Value	Units
number of time steps	25	-
number of cells x- and y-dir (n)	200	-
model size in x- and y-dir (l)	600	m
shale permeability (k_I)	1e-19	m^2
damage permeability (k_D)	1e-8	m^2
porosity (ϕ)	0.15	-
injection rate (Q)	60	$\mathrm{m}^3\,\mathrm{h}^{-1}$
simulation time (t_{end})	24	h
least comp. stress (σ'_h)	25	MPa
eff. compressibility (α_D)	1e-8	Pa^{-1}
max strength ($s_{\max}$)	10	MPa

Table 1: The parameters used in the reference case.

the parameters in table 1, which serves as a reference case. Common for all cases is an isotropic stress state in the plane. The fracture condition is that the fluid pressure must exceed the least compressive stress plus the bond strength in a cell. The bond strength has a uniform distribution of random values in the interval from zero to $s_{\max} = 10$ MPa. The effective compressive stress is $\sigma'_h = 25$ MPa, which is the least compressive stress minus the hydrostatic fluid pressure. It could, for example, be the stress state at 2 km depth, assuming that the vertical stress is the largest principal stress.

Figure 3 shows how the damaged rock volume develops in case of a damaged rock permeability of $k_D = 1 \cdot 10^{-8}$ m^2. The damaged rock volume propagates away from the injection point as a structure that appears similar to a percolation network. The growth of the damage zone takes place in random directions by addition of clusters of different sizes. Each microseismic event is a cluster, and the clusters are not dense. A particular feature of the network is that it has no loops. The fracture branches do not reconnect to form loops, as seen from figure 4. It should be mentioned that the no-loop feature is built into the model, and it is not the result of a parameter choice. The large permeability of the damaged rock accounts for the dilation of the damage zone due to the fluid pressure exceeding the least compressive stress. When this value is used with a parallel plate model for fracture permeability it gives a plate separation of 0.3 mm. The large permeability implies a low pressure difference between the injection cell and the perimeter cells of the damaged area. Some bonds have a sufficiently high strength to remain intact.

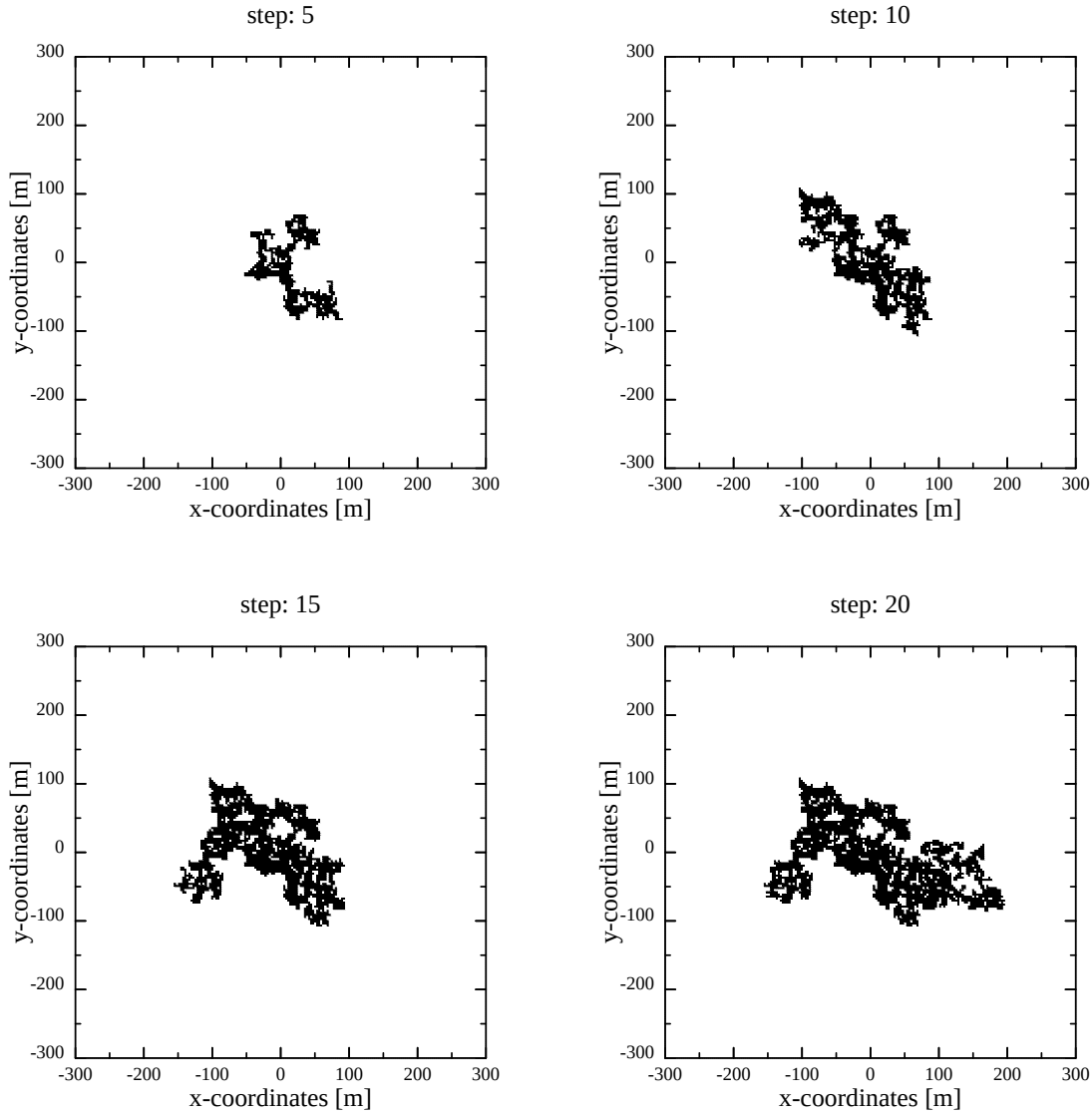

Figure 3: *The development of the damaged rock zone is plotted at four different time steps for the case of an isotropic stress state in the xy-plane. The figure shows how the volume of damaged rock has propagated randomly in different directions after addition of clusters of different sizes. Furthermore, the zone of damaged rock is not dense, but it has holes. The damaged rock appears similar to a percolation cluster at each time step. The final stage (time step 25) is plotted in figure 4.*

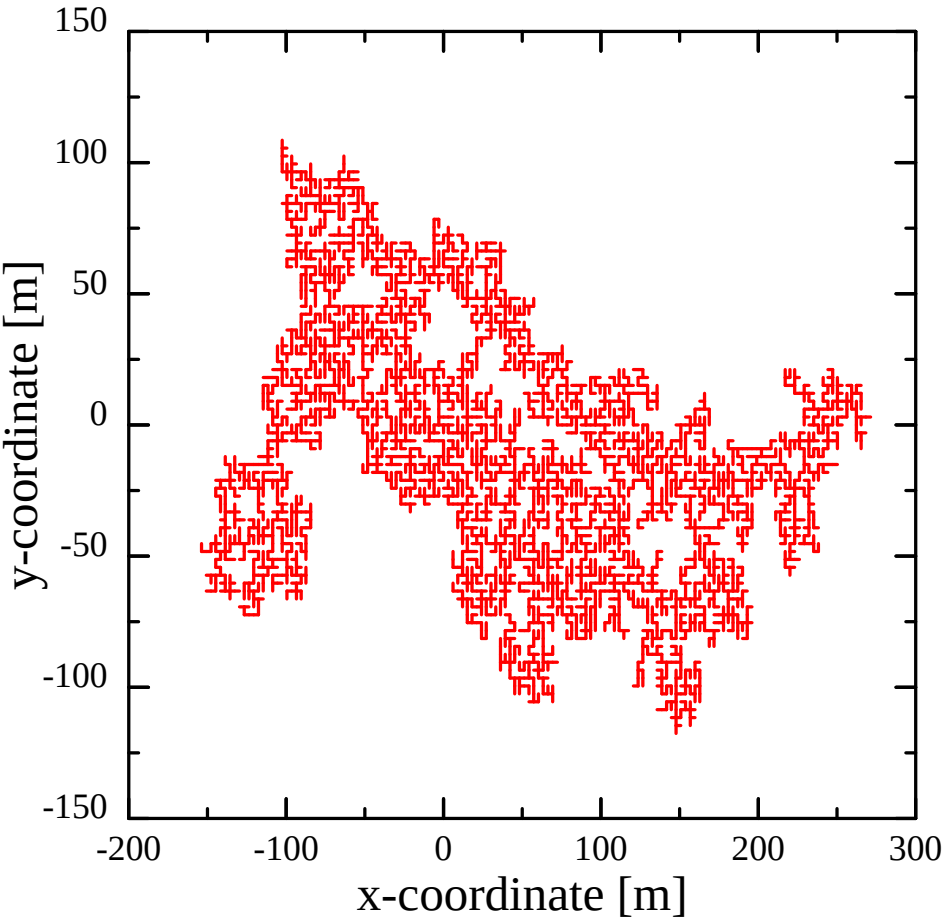

Figure 4: *The broken bonds that constitute the network of damaged cells at the end of the simulation. Each bond connects two damaged cells, and there are no loops in the network.*

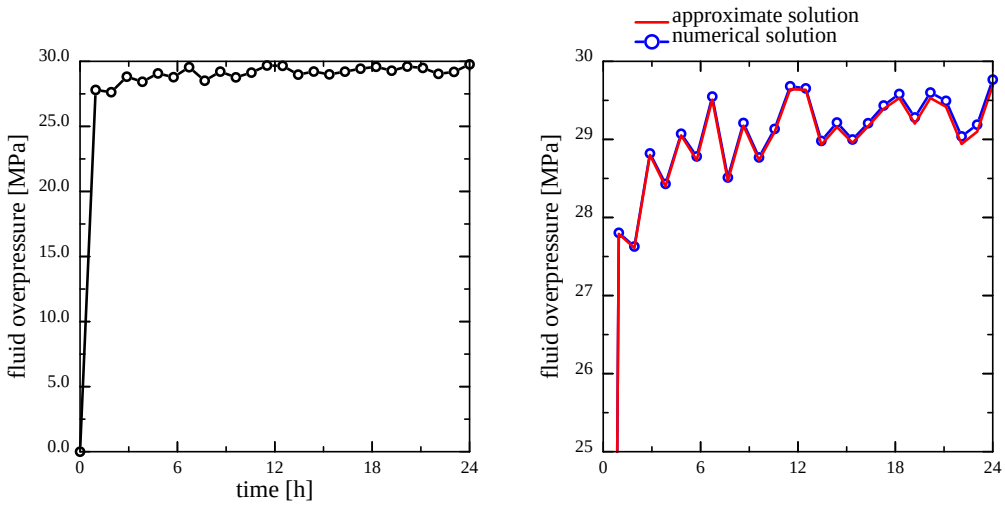

Figure 5: *(a) The injection fluid pressure as a function of time. (b) A closer look at the oscillations in plot (a).*

The injection pressure is plotted in figure 5 as a function of time. The fluctuations are due to the random strength of the bonds. There is a slight trend of increasing fluid pressure, which is related to the increasing distance to the rim of the damaged zone. The numerical solution is compared with the stationary solution in figure 5, and they are close. This is because the permeability is sufficiently high in the damage zone to make the characteristic time for the decay of transients, given by equation (4), short compared with the injection time. The time constant is only $t_0 = 1.5$ s when $r_{\max} = 100$ m, and the compressibility and the viscosity are taken from table 1.

Figure 6 shows how the events are distributed on the grid. The colour of the circles gives the time of the events, and the ball size shows the size of the events. The colours show that the damage zone expands first up and down, then to the left and finally to the right. The damage zone develops quite differently from a circular expansion away from the injection point. The events are plotted in figure 7a as they appear in time. Events of different sizes seem uniformly distributed in time. The events are plotted by their radial distance from the well as a function of time in figure 7b. The plot indicates a depletion of events in the near well zone after $t = 14$ h. The elements that remain intact near the injection cell are connected with bonds that are too strong relative to the injection pressure. The events may be limited in space and time by a front and a back front, as demonstrated by Shapiro

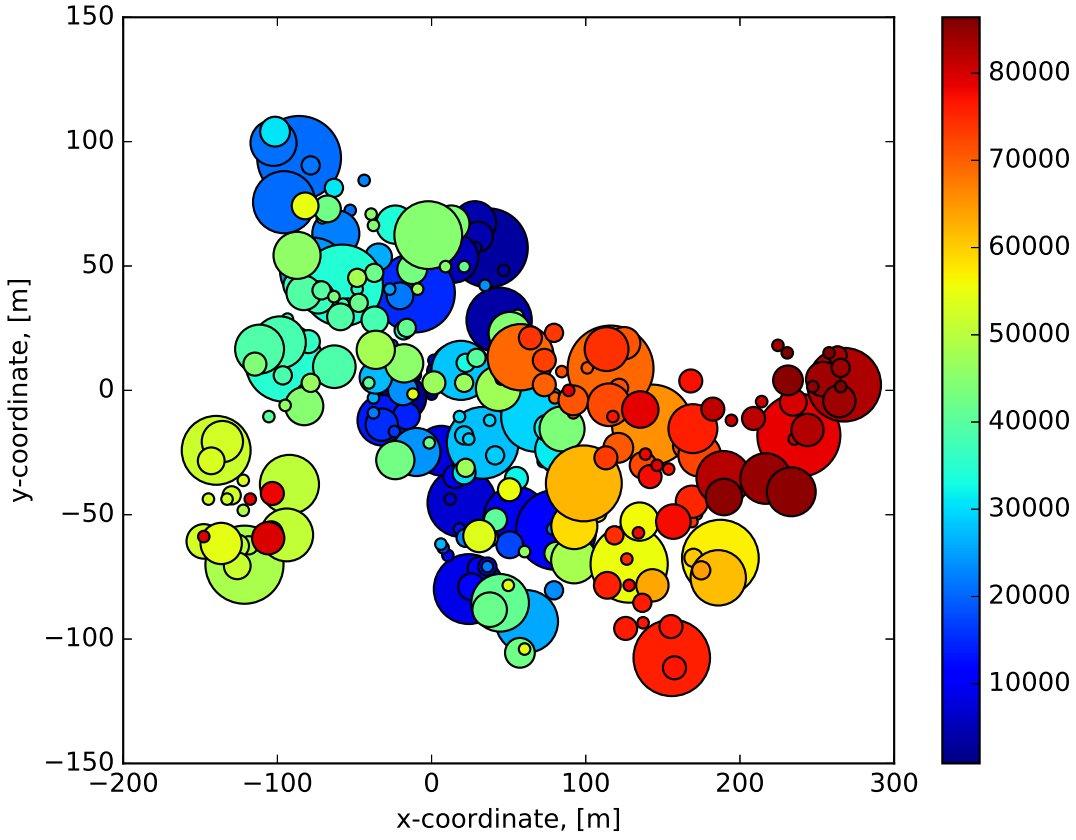

Figure 6: *The event magnitudes in the xy-space. The size of the circles reflects the size of the events and the colour the time of the event.*

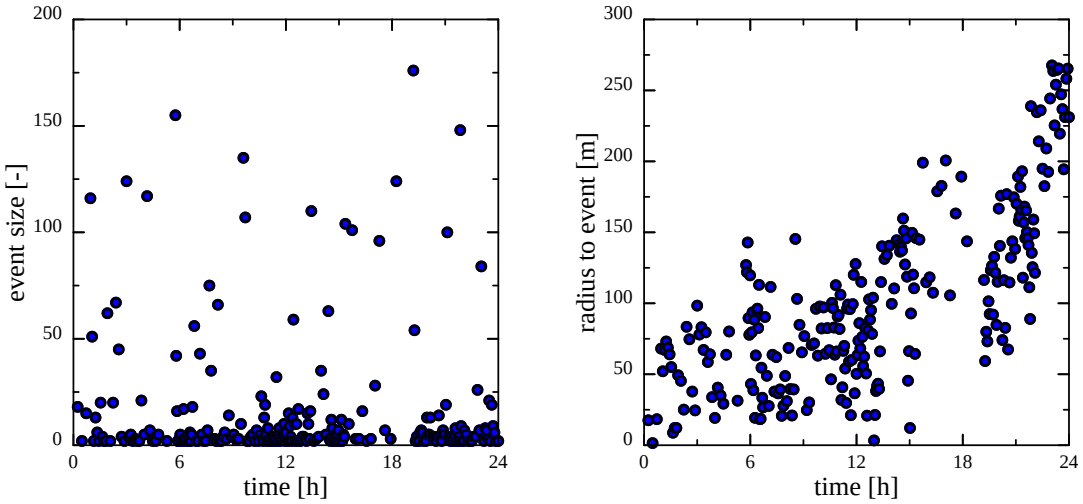

Figure 7: *(a) The event sizes as a function of time. (b) The event radius (distance from well) as a function of time.*

et al. (1997) and Rothert and Shapiro (2003), where both fronts may increase proportional to $t^{1/2}$. The front delimits where the damage zone propagates into the intact rock, and the back front marks the area that is depleted of microseismicity. The events in figure 7b are too scattered to allow for the fitting of a precise curve for the front and the back front.

8 Magnitude and frequency of events

The magnitude of an event with size S is

$$M = \log_{10} S, \tag{7}$$

where the size S is the number of broken cells. Therefore, the size of an event is proportional to the area of the damaged rock in 2D or the volume of the damaged rock in 3D. Our model with loop-less fracture branches has the same number of broken bonds as broken cells. The percolation model of Norris et al. (2014b,a) defines the event size as the number of broken bonds. The frequency-magnitude of microseismicity often follows the linear Gutenberg–Richter relation (Crampin

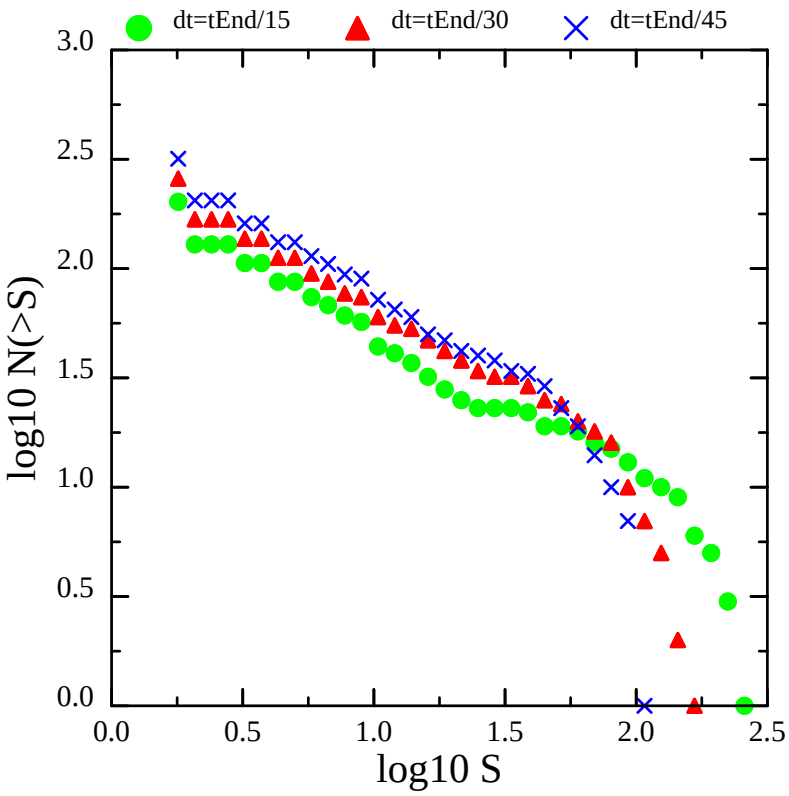

Figure 8: *The frequency-magnitude distribution's dependence on the time step. The different time steps are* $dt = 1.6$ *h,* 0.47 *h and* 0.53 *h, respectively.*

and Gao, 2015)

$$\log_{10} N = a - bM, \tag{8}$$

where N is the number of events greater than or equal to a given magnitude M, and where a and b are empirical parameters. The parameter a gives a reference level, while the b value is the slope of the line. A high b value indicates a larger proportion of small events relative to large events, and lower a b value represents the opposite – a smaller proportion of small events relative to large events. The b value is observed for earthquakes from different regions to be in the range of $0.8 < b < 1.2$ (Turcotte, 1997).

The time step is a numerical parameter in the model and not a physical parameter. Figure 8 shows the frequency-magnitude relation for the three different number of time steps 15, 25 and 45, and the other parameters are from table 1. The reference case has 25 time steps. We see from figure 8 that the b-value is insensitive for reasonable choices of time step. All three cases have approximately 0.8 as b value, a value that is towards the lower end of what is observed. Urban et al. (2016) reports b values as low as 0.75 measured during the filling of the Song Tranh dam in Vietnam. On the other hand, hydraulic fracturing has been characterized by b values close to 2 (Eaton et al., 2014; Eaton and Maghsoudi, 2015). Norris et al. (2014a) obtained the b value $b \approx 0.46$ with their 2D loop-less percolation model. They commented that extending the model from 2D to 3D might change the b value.

The definition of the magnitude implies that the fracture surface (2D) or volume (3D) has a power-law size distribution, at least over the linear part of the frequency-magnitude interval. The lowest possible magnitude is zero, as it is just one broken cell. It is possible to estimate an upper limit of the event size. From equation (5) it follows that the damaged volume created during a time step Δt can be estimated as

$$\Delta V_D = \frac{Q\,\Delta t}{\phi\,\alpha_D\,p_{\text{av}}}, \tag{9}$$

where p_{av} is the average overpressure in the damaged rock. The average overpressure can be approximated as $p_{\text{av}} \approx \sigma'_h$, when p_{av} is only slightly larger than the effective least compressive stress. The largest possible event takes place when the damaged volume ΔV_D forms one single cluster. The approximation of the maximum size for the one-cluster-event becomes

$$S_{\max} \approx \frac{\Delta V_D}{V_{\text{cell}}} = \frac{Q\,\Delta t\,n^2}{\phi\,\alpha_D\,\sigma'_h\,l^2}, \tag{10}$$

where the volume of a 2D grid cell is $V_{\text{cell}} = (l/n)^2$, and where l and n are the grid size and the number of cells in the x- and y-directions, respectively. The max

cluster size (10) is also an upper bound on the cluster size because $p_{\mathrm{av}} > \sigma'_h$. The parameters for the reference case (table 1), gives that $S_{\max} = 178$ and $M_{\max} = \log_{10}(S_{\max}) = 2.25$. Figure 8 shows that the largest event for the reference case has a magnitude close to $M_{\max} = 2.25$. Estimate (10) gives that the maximum size of an event is proportional to the time step and inversely proportional to the grid size when $p_{\mathrm{av}} \approx \sigma'_h$. Figure 8 shows that increasing the time step gives a longer tail with larger events. The span in magnitudes is therefore in the range from 0 to 2.25 for the cases in figure 8. The linear segment of the frequency-magnitude plot is shorter and covers the range from 0.25 to 2.0.

The grid resolution is also a numerical parameter and it defines the size of the smallest unit of rock that can be damaged during a time step. Figure 9 shows how the simulation results depend on the grid resolution. The case with 200×200 cells is the reference case. The two other cases are the same, except that one is coarser with 100×100 cells and one is finer with 300×300 cells. The coarse case has fewer large events than the cases with finer grid resolution, as expected from estimate (10) for the maximum event size. The linear part of the frequency-magnitude distribution has a less steep slope than the reference case. Therefore, the b value varies slightly with the grid size, at least in the range of grid sizes shown. Although the b-value is only weakly sensitive to the grid resolution, the number of damaged cells in the largest events depends on the grid resolution.

Figure 10 demonstrates how the frequency-magnitude distribution depends on the bond strength. The figure shows cases where the bond strength is both reduced and increased with one order of magnitude relative to the reference case. The slope of the linear part of the curves is the same. Reducing the bond strength gives more events, since weak bonds are easier to break, but the b-value of the frequency-magnitude distribution is nearly the same.

The damage permeability is an important parameter for the frequency-magnitude distribution of the events. Increasing the damage permeability brings the fluid pressure closer to the stationary pressure. The fluid pressure of the reference case is already close to the stationary pressure, as seen from figure 5b. Increasing the damage permeability further does not change the results very much. Figure 11a shows the reference case compared with cases where the damage permeability is reduced by 2 and 4 orders of magnitude. It is seen that reducing the permeability reduces the number of large events, and that the slope of the frequency-magnitude distribution becomes steeper and less linear. A smaller damage permeability implies that there is a larger injection pressure and a larger pressure gradient over the damaged cells, along the fracture branches, as seen in figure 11b. A larger pressure gradient implies that the damage zone spreads out from the injection point circularly, as shown in figure 12a. The pressure is too high for bonds and cells to

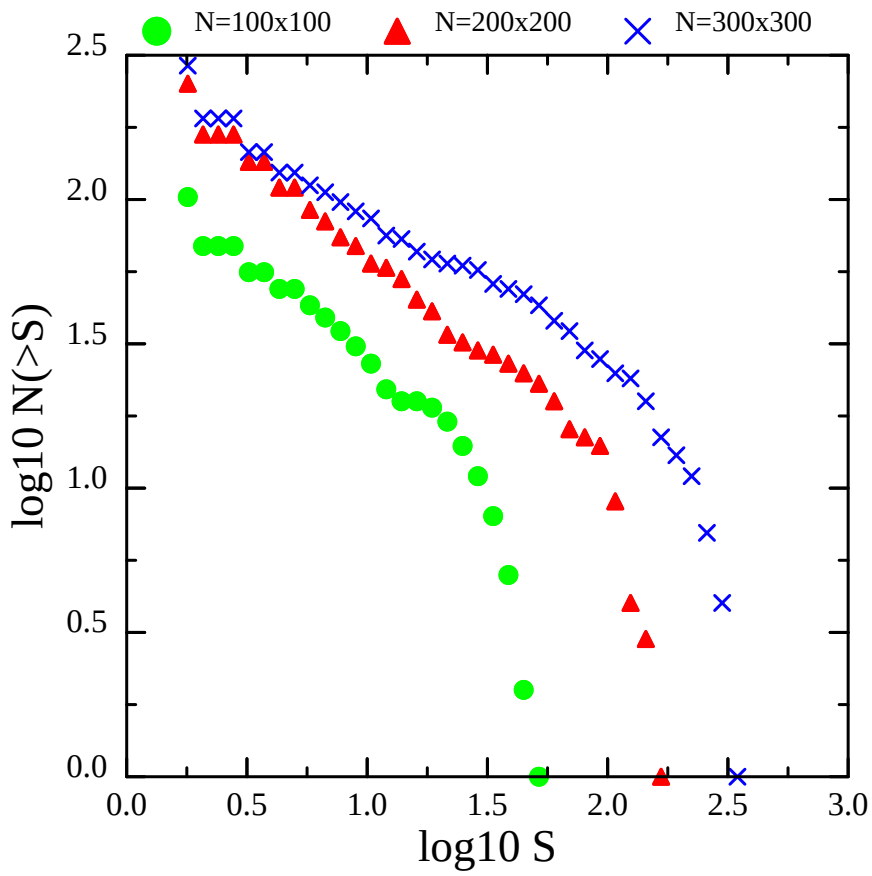

Figure 9: *The plot show how the frequency-magnitude distribution depends on the grid resolution.*

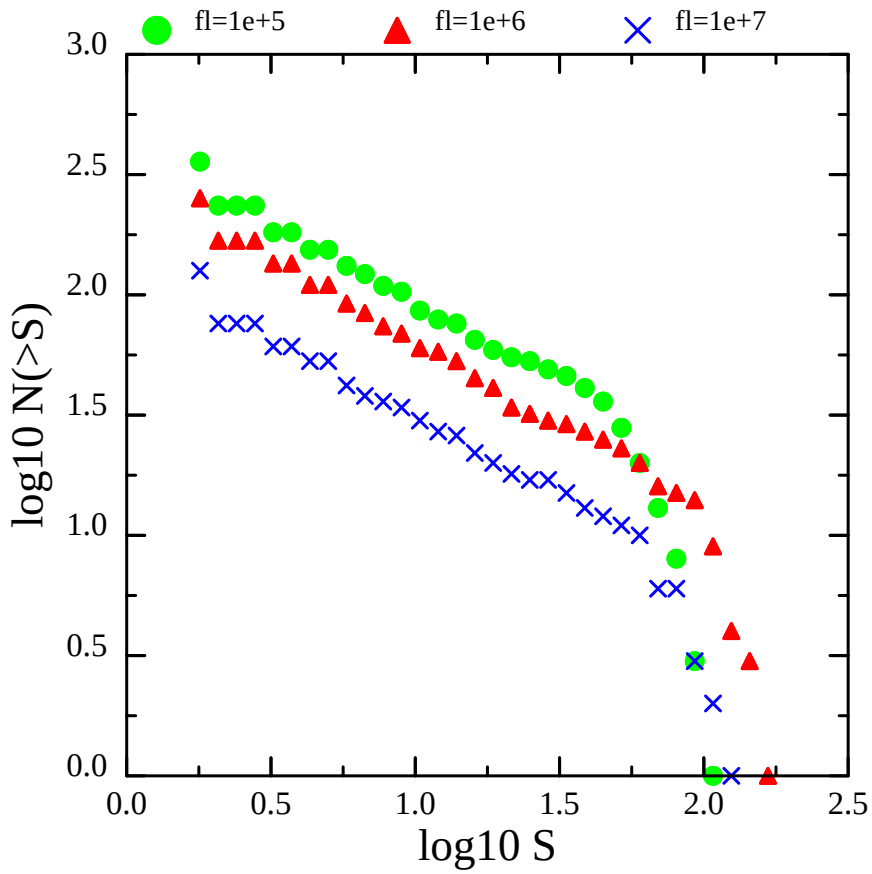

Figure 10: *The plot show how magnitude distribution depends on the strength.*

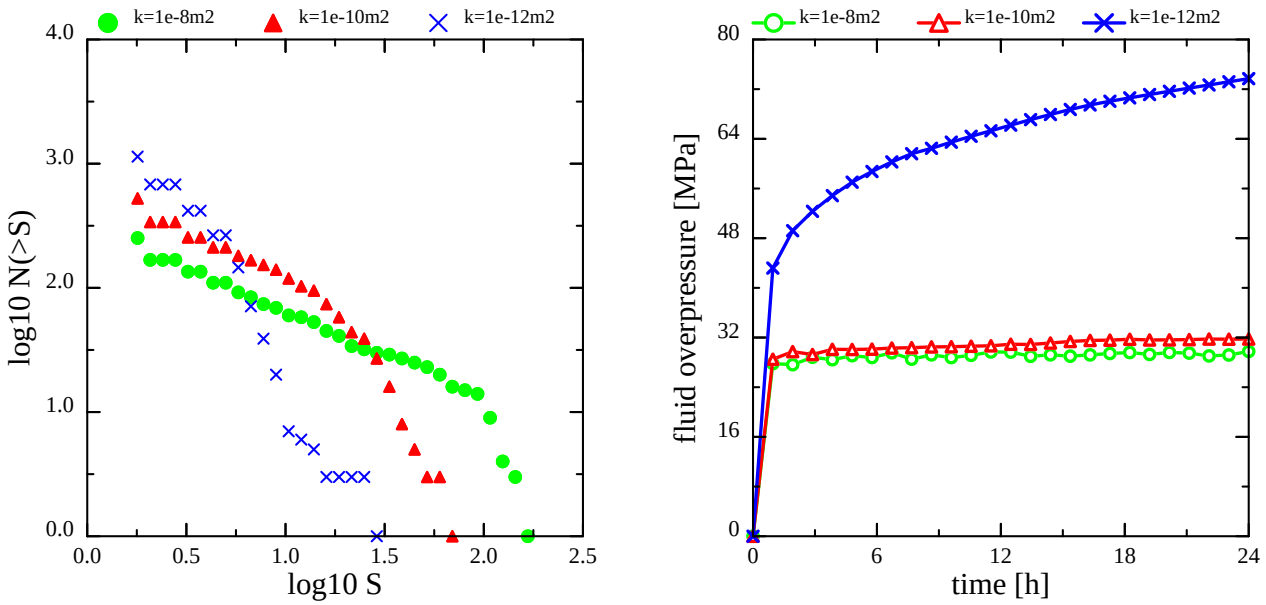

Figure 11: *The permeability of the damage rock has an impact on the magnitude distributions. (a) The magnitude distribution's dependence on the damage permeability. (b) The injection pressure corresponding to the magnitude distributions in (a).*

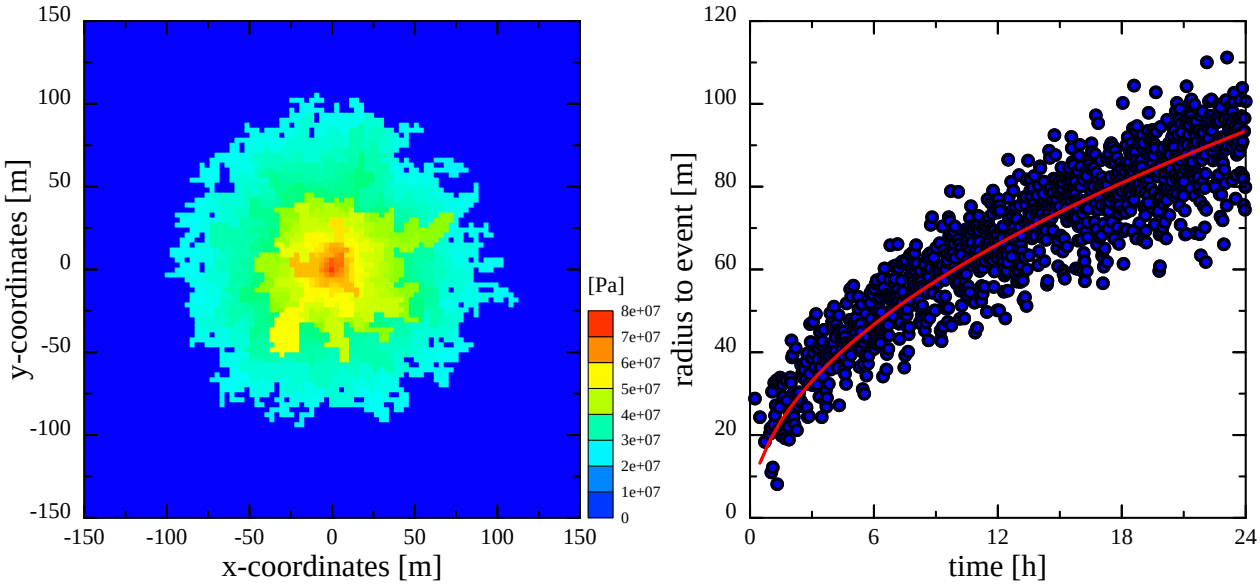

Figure 12: *(a) The pressure distribution in the damaged rock at the end of the simulation of the case* $k_D = 1 \cdot 10^{-12}$ m^2 *from figure 11. The units for pressure are Pa. (b) Radius as a function of the time for the events. The red curve is the radius, equation (6), for the average pressure* $p_{\mathrm{av}} = 35$ *MPa.*

remain intact inside the near-well area. The events form a band in space and time, as seen from figure 12b, where the band shows the front and the back front of the circular expansion of the damage process. The radius (6) is plotted for the average pressure $p_{\rm av} = 35$ MPa, and it is a good estimate of the average front position of the damaged rock.

9 Conclusion

A model is suggested for the simulation of hydraulic fracturing and damage of low permeable rock, which is an extension of the percolation model developed by Norris et al. (2014b) and Norris et al. (2016). The model is based on a regular grid of cells, where the cell centers are connected by transmissibilities, also called bonds. The bonds have strength and can break. Breaking a bond also breaks (or damage) the intact cell it is connected to. The condition for breaking a bond is that the fluid pressure exceeds the least compressive stress and the random bond strength. The bond strength is uniformly distributed between 0 and a maximum strength.

Damaged cells become permeable. The permeability of the damaged rock is high, because the fluid pressure exceeds the least compressive stress, and therefore, opens the rock. The model solves for the fluid pressure after each breaking of a bond, and the fluid pressure decreases slightly when it invades a newly broken cell. The model computes the injection pressure and how it fluctuates with the propagation of the damaged cells.

The model also computes the fracture network of damaged cells and thereby the bulk volume of stimulated rock. The fracture network has non-connected branches (it is loop-less). Broken bonds that belong to the same cluster during a time step constitute an event. The size of the event is the number of damaged cells in the cluster, which is also the same as the number of broken bonds for non-connected branches. These events create the microseismicity, where the magnitude is the $\log_{10}$ of the event size. The model computes the space-time distribution of the events as well as their magnitudes during the propagation of the damage zone.

Gutenberg–Richter plots produced by the model show frequency-magnitude distributions having linear trends when the damaged rock has sufficiently high permeability for pressure gradients to be small. These cases of "high" permeability have b values being approximately 0.8. A simple estimate is derived for the maximum magnitude. The largest magnitudes in the current study using relative coarse grids are 2.5, which is close to the estimated maximum magnitude. The smallest

events are only one cell large and have magnitude of 0.

The damage model is tested with respect to the numerical parameters time step and grid size. A long time step allows for more events than a short time step, because more fluid is injected during a long time step and a larger damaged rock volume is needed to host the fluid increment. The model is not sensitive to the time step, since reasonable differences in the time step give nearly the same b-value. The grid size (element size) defines the size of the least possible event. The number of damaged cells in the largest events increases with a finer grid size, but the b-value for different grid sizes are nearly the same.

The model is studied with respect to the physical parameters rock strength and the permeability of the damaged rock. The microseismic event distribution is tested for a span of rock strengths and we found that the b-value remained nearly unchanged. On the other hand, the permeability of damaged rock controls how the damage process propagates. There are two different types of behaviour of the model with respect to the permeability. The damaged rock volume resembles a percolation cluster when the permeability is sufficiently high for pressure gradients to be small. In the other regime, for "moderate" permeabilities that gives noticeable pressure gradients, the damaged rock volume propagates outwards in a circular manner. The injection pressure increases substantially beyond the fracturing level for "moderate" permeabilities. Furthermore, the steepness of the linear trends increases, and thereby the b values, with decreasing permeability of the damaged rock.

The proposed model produces a realistic frequency-magnitude distribution of microseismicity. The model is straightforward to extend to 3D and can be developed further with a number of additional features such as different breaking conditions, improved modules for damage permeability, anisotropic stress fields and by allowing hydraulically connected fracture branches.

10 Appendix: Finite volume formulation

Conservation of fluid mass is expressed as

$$\frac{\partial(\phi\varrho)}{\partial t} + \nabla \cdot (\varrho \mathbf{v}) = 0, \tag{11}$$

where $\mathbf{v} = -(k/\mu)\nabla p$ is the Darcy flux and ϱ is the fluid density. Introduction of the effective compressibility

$$\alpha = \frac{1}{(\phi\varrho)}\frac{\partial(\phi\varrho)}{\partial p}, \tag{12}$$

gives pressure equation (1). The effective compressibility is a simple mean to represent the combined compressibility of the rock and fluid. A finite volume formulation is obtained from the conservation law for fluid (11) by integration over a cell volume V_i

$$\int_{V_i}\frac{\partial(\phi\varrho)}{\partial t}dV = -\int_{V_i}\nabla\cdot(\varrho\mathbf{v})\,dV = -\oint_{A_i}\varrho\,\mathbf{v}\cdot\mathbf{n}_i\,dA. \tag{13}$$

The last equality is obtained by the divergence theorem, which takes the volume integral to a surface integral over the cell volume, where A_i is the surface area and $\mathbf{n}_i$ is outward unit vector of cell i, respectively. The surface integral is replaced by the sum over the four sides of the 2D cell V_i. The discrete version of integral equation (13) becomes

$$\phi_i\alpha_i\frac{(p_i^n - p_i^{n-1})}{\Delta t}V_i = \sum_{j\in<i>}A_{ij}\frac{k_{ij}}{\mu}\frac{(p_j^n - p_i^n)}{l_{ij}}, \tag{14}$$

where subscript i indicates that the property is in cell i. The sum over $j \in< i >$ is all four nearest neighbour cells j of cell i. The common area of the interface between cell i and j is denoted as A_{ij}, and the distance from the cell center i to cell center j is l_{ij}. The harmonic average permeability of the two nearest neighbour cells i and j is k_{ij}. Therefore, the Darcy flux from cell i to cell j is $v_{ij} = (k_{ij}/\mu)(p_i^n - p_j^n)/l_{ij}$. Pressure equation (14) is made implicit in pressure using a backward Euler time discretisation, where the superscripts n and $n-1$ denote the current and the previous time step, respectively. The transmissibility between cell i and j is

$$T_{ij} = \frac{A_{ij}k_{ij}}{l_{ij}}, \tag{15}$$

which gives the hydraulic coupling between the cells.

11 Acknowledgement

The author is grateful to Andreas Wuestefeld for his comments to the manuscript. Parts of this work have been supported by the Research Council of Norway through the project 244570/E30 “StressLess” and Statoil. The conclusions of the paper are not necessarily the opinions of Statoil.

12 References

References

Aker, E., Jørgen Måløy, K., Hansen, A., Batrouni, G., 1998. A two-dimensional network simulator for two-phase flow in porous media. Transport in Porous Media 32, 163–186.

Amitrano, D., 2003. Brittle-ductile transition and associated seismicity: Experimental and numerical studies and relationship with the b value. Journal of Geophysical Research 108, 1–15.

Amitrano, D., 2006. Rupture by damage accumulation in rocks. International Journal of Fracture 139, 369–381.

Amitrano, D., 2012. Variability in the power-law distributions of rupture events. The European Physical Journal - Special Topics 205, 199–215.

Baan, M.v.d., Eaton, D., Dusseault, M., 2013. Microseismic monitoring developments in hydraulic fracture stimulation, in: Bunger, A.P., McLennan, J., Jeffrey, R. (Eds.), Effective and Sustainable Hydraulic Fracturing. InTech, Rijeka. chapter 21.

Bak, P., Tang, C., Wiesenfeld, K., 1987. Self-organized criticality: An explanation of the 1/f noise. Phys. Rev. Lett. 59, 381–384.

Bruel, D., 2007. Using the migration of the induced seismicity as a constraint for fractured hot dry rock reservoir modelling. International Journal of Rock Mechanics and Mining Sciences 44, 1106–1117.

Bruel, D., Charlety, J., 2007. Moment-frequency distribution used as a constraint for hydro-mechanical modelling in fracture networks, in: International Society for Rock Mechanics, 11th ISRM Congress, Portugal, Lisbon, Portugal. pp. 1–5.

Busetti, S., Mish, K., Hennings, P., Reches, Z., 2012a. Damage and plastic deformation of reservoir rocks: Part 2. Propagation of a hydraulic fracture. AAPG Bulletin 96, 1711–1732.

Busetti, S., Mish, K., Reches, Z., 2012b. Damage and plastic deformation of reservoir rocks: Part 1. Damage fracturing. AAPG Bulletin 96, 1687–1709.

Crampin, S., Gao, Y., 2015. The physics underlying Gutenberg-Richter in the earth and in the moon. Journal of Earth Science 26, 134–139.

Eaton, D.W., Davidsen, J., Pedersen, P.K., Boroumand, N., 2014. Breakdown of the Gutenberg-Richter relation for microearthquakes induced by hydraulic fracturing: influence of stratabound fractures. Geophysical Prospecting 62, 806–818.

Eaton, D.W., Maghsoudi, S., 2015. 2b... or not 2b? Interpreting magnitude distributions from microseismic catalogs. First Break 33, 79–86.

Flekkøy, E.G., MaltheSørenssen, A., Jamtveit, B., 2002. Modeling hydrofracture. Journal of Geophysical Research: Solid Earth 107(B8), 1–11.

Furuberg, L., Feder, J., Aharony, A., Jøssang, T., 1988. Dynamics of invasion percolation. Physical Review Letters 61, 2117–2120.

Furuberg, L., Måløy, K.J., Feder, J., 1996. Intermittent behavior in slow drainage. Phys. Rev. E 53, 966–977.

Ghani, I., Koehn, D., Toussaint, R., Passchier, C.W., 2013. Dynamic development of hydrofracture. Pure and Applied Geophysics 170, 1685–1703.

Itasca International, I., 2016. Universal Distinct Element Code (UDEC), Version 6.0, http://www.itascacg.com/software/udec.

Izadi, G., Elsworth, D., 2014. Reservoir stimulation and induced seismicity: Roles of fluid pressure and thermal transients on reactivated fractured networks. Geothermics 51, 368–379.

Langenbruch, C., Shapiro, S.A., 2014. Gutenberg-Richter relation originates from Coulomb stress fluctuations caused by elastic rock heterogeneity. Journal of Geophysical Research: Solid Earth 119, 1220–1234.

Maxwell, S.C., Mack, M., Zhang, F., Chorney, D., Goodfellow, S.D., Grob, M., 2015. Differentiating wet and dry microseismic events induced during hydraulic theory of shear failure, URTeC: 2154344, in: Proceedings of Unconventional Resources Technology Conference, Unconventional Resources Technology Conference, San Antonio, Texas. pp. 1–12.

Miller, S., Nur, A., 2000. Permeability as a toggle switch in fluid-controlled crustal processes. Earth and Planetary Science Letters 183, 133–146.

Neuzil, C., 1994. How permeable are clays and shales. Water Resources Research 30, 145–150.

Niebling, M.J., Toussaint, R., Flekkøy, E.G., Måløy, K.J., 2012. Dynamic aerofracture of dense granular packings. Physical Review E 86, 061315.

Norris, J.Q., Turcotte, D.L., Rundle, J.B., 2014a. Anisotropy in fracking: A percolation model for observed microseismicity. Pure and Applied Geophysics 172, 7–21.

Norris, J.Q., Turcotte, D.L., Rundle, J.B., 2014b. Loopless nontrapping invasion-percolation model for fracking. Phys. Rev. E 89, 022119.

Norris, J.Q., Turcotte, D.L., Rundle, J.B., 2016. Fracking in tight shales: What is it, what does it accomplish, and what are its consequences? Annual Review of Earth and Planetary Sciences 44, 321–351.

Riahi, A., Damjanac, B., 2013. Numerical study of hydro-shearing in geothermal reservoirs with a pre-existing discrete fracture network, in: Proceedings, Thirty-Eighth Workshop on Geothermal Reservoir Engineering, Stanford University, California. pp. 1–13.

Rothert, E., Shapiro, S.A., 2003. Microseismic monitoring of borehole fluid injections: Data modeling and inversion for hydraulic properties of rocks. Geophysics 68, 685–689.

Shapiro, S.A., Dinske, D., Rothert, E., 2006. Hydraulic-fracturing controlled dynamics of microseismic clouds. Geophysical Research Letters 33, 1–5.

Shapiro, S.A., Huenges, E., Borm, G., 1997. Estimating the crust permeability from fluid-injection-induced seismic emission at the KTB site. Geophysical Journal International 131, F15–F18.

Spence, D.A., Turcotte, D.L., 1985. Magma-driven propagation of cracks. Journal of Geophysical Research-Solid Earth and Planets 90, 575–580.

Taron, J., Elsworth, D., Min, K.B., 2009. Numerical simulation of thermal-hydrologic-mechanical-chemical processes in deformable, fractured porous media. International Journal of Rock Mechanics and Mining Sciences 46, 842–854.

Turcotte, D., Moores, E., Rundle, J., 2014. Super fracking. Physics Today 67, 34–39.

Turcotte, D.L., 1997. Fractals and Chaos in Geology and Geophysics. Cambridge University Press, Cambridge. 2nd edition. 398 pp.

Tzschichholz, F., Herrmann, H., 1995. Simulations of pressure fluctuations and acoustic emission in hydraulic fracturing. Phys. Rev. E 51, 1961–1970.

Tzschichholz, F., Herrmann, H., Roman, H., Pfuff, M., 1994. Beam model for hydraulic fracturing. Phys. Rev. B 49, 7056–7059.

Tzschichholz, F., Wangen, M., 1998. Modelling of hydraulic fracturing of porous materials. WIT Press, Southhampton. chapter 8. pp. 227–260.

Urban, P., Lasocki, S., Blascheck, P., do Nascimento, A.F., Van Giang, N., Kwiatek, G., 2016. Violations of Gutenberg-Richter Relation in Anthropogenic Seismicity. Pure and Applied Geophysics 173, 1517–1537.

Verdon, J.P., Stork, A.L., Bissell, R.C., Bond, C.E., Werner, M.J., 2015. Simulation of seismic events induced by CO2 injection at In Salah, Algeria. Earth and Planetary Science Letters 426, 118–129.

Wangen, M., 2011. Finite element modelling of hydraulic fracturing on a reservoir scale in 2d. Journal of Petroleum Science and Engineering 77, 274–285.

Wangen, M., 2013. Finite element modeling of hydraulic fracturing in 3d. Computational Geosciences 17, 647–659.

Wilkinson, D., Willemsen, J.F., 1983. Invasion percolation: a new form of percolation theory. J. Phys. A: Math. Gen 16, 3365–3376.

Zoback, M.D., 2010. Reservoir geomechanics. Cambridge University Press.